

Fig. 5. The differences between the exact value of the x -component of the H -field and the numerically approximated.

Mur ABC is placed far away from the source so that it yields the same accuracy as does the nonlocal ABC, it required approximately a third of the CPU time. In this latter case, however, the computer memory requirement of the Mur ABC was orders of magnitude more than the requirements of the nonlocal ABC. Hence, it is difficult to make general statements regarding which type of ABC is computationally more effective. In any event it is clear that research should be directed at finding ways of improving the CPU time required by the nonlocal ABC's if they are to be used instead of the usual local ABC's.

IV. CONCLUSIONS

The exact nonlocal ABC derived in [8] appears to be a useful and accurate tool to implement a nonreflecting ABC for the FDTD method. The accuracy is better than the nonlocal ABC of [9] since this formulation allows higher order interpolation and integration which is not possible with the approach of [9]. When the accuracy of the current method and the local type of ABC's such as those due to Mur are required to be the same, the nonlocal ABC requires significantly less computer memory than does the Mur type ABC, but more CPU time than the Mur ABC.

Our method may be implemented with any order interpolation and integration schemes, so that we may increase the accuracy further if so desired with little computational overhead. This is in contrast to the method of [9] which is first order accurate. Research at reducing the CPU time requirements is continuing.

REFERENCES

- [1] K. S. Yee, "Numerical solution of initial boundary value problems involving Maxwell's equations in isotropic media," *IEEE Trans. Antennas Propagat.*, vol. AP-14, no. 3, pp. 302-307, May 1966.
- [2] A. Bayless and E. Turkel, "Radiation boundary conditions for wave-like equations," *Pure Applied Math.*, vol. XXXIII, pp. 707-725, 1980.
- [3] B. Engquist and A. Madja, "Absorbing boundary conditions for the numerical simulation of waves," *Math. of Computation*, vol. 31, no. 139, pp. 629-651, July 1977.
- [4] G. Mur, "Absorbing boundary conditions for the finite difference approximation of the time-domain electromagnetic field equations," *IEEE Trans. Electromag. Compat.*, vol. EMC-23, no. 4, pp. 377-382, Nov. 1981.
- [5] B. Gustafsson and H. O. Kreiss, "Boundary conditions for time dependant problems with an artificial boundary," *J. Comput. Phys.*, vol. 30, pp. 333-351, 1979.
- [6] T. G. Moore, J. G. Blashak, A. Tavlove, and G. A. Kriegsmann, "Theory and applications of radiation boundary operators," *IEEE Trans. Antennas Propagat.*, vol. AP-36, no. 12, pp. 1797-1811, Dec. 1988.
- [7] J. B. Keller and D. Govoli, "Exact non-reflecting boundary conditions," *J. Computat. Phys.*, vol. 82, pp. 172-192, 1989.
- [8] J. C. Olivier, "On the synthesis of exact free space absorbing boundary conditions for the finite difference time domain method," *IEEE Trans. Antennas Propagat.*, vol. 40, no. 4, pp. 456-460, Apr. 1992.
- [9] J. De Moerloose and D. de Zutter, "Surface integral representation radiation boundary conditions for the FDTD method," *IEEE Trans. Antennas Propagat.*, vol. 41, no. 7, pp. 890-896, July 1993.
- [10] L. Ting and M. J. Miksis, "Exact boundary conditions for scattering problems," *J. Acoust. Soc. Amer.*, vol. 80, pp. 1825-1827, 1986.
- [11] O. M. Ramai and R. Mittra, "Finite element solution for a class of unbounded geometries," *IEEE Trans. Antennas Propagat.*, vol. 39, no. 2, Feb. 1991.
- [12] A. Tavlove and M. E. Brown, "Numerical solution of steady-state electromagnetic scattering problems using the time-dependant Maxwell's equations," *IEEE Trans. Microwave Theory Tech.*, vol. MTT-23, no. 8, pp. 623-630, Aug. 1975.

Superspheroids: A New Family of Radome Shapes

P. L. Overfelt

Abstract—In the following we use the arc described by the two-dimensional superquadric equation (taking its exponent ν to be any positive real number) in the first quadrant only and revolve it about its major axis to obtain a body of revolution family of geometric shapes called superspheroids. For certain values of length and radius and assuming that $1 < \nu < 2$, we have determined new shapes that are appropriate for high speed missile radomes. We have found that the superspheroid with optimized exponent value $\nu = 1.381$ can almost exactly reproduce the traditional Von Karman radome geometry. Incidence angle maps and geometric properties have been determined for this superspheroidal family. We have used a ray tracing analysis to obtain boresight error induced by this family of shapes as a function of gimbal angle. The superspheroids are mathematically simple, can approximate most of the traditional radome geometries quite well, and are exceptionally easy to either program or use analytically.

I. INTRODUCTION

The two-dimensional superquadric equation [1]

$$(x/a)^\nu + (y/b)^\nu = 1 \quad (1)$$

has been applied recently to electromagnetic problems in the context of scattering from perfectly conducting superquadric cylinders [2] and also in the analysis of reflector antennas with superquadric aperture boundaries [3]. Generally x and y in (1) are assumed to run over the intervals $-a \leq x \leq a$, $-b \leq y \leq b$. In the following we write (1) in the form

$$y = (b/a)(a^\nu - x^\nu)^{1/\nu}, \quad (2)$$

$b \leq a$, ν any positive real number, and we keep in mind that in taking the ν th root, we are interested in real roots only. In (2) we allow x to take on positive values only, i.e., $0 \leq x \leq a$. In this case (2) is an arc in the xy plane which is completely above the x -axis except at the end point, $x = a$. By taking this arc, $y = f(x) \geq 0$, and revolving it about the x -axis, we obtain a body of revolution (BOR) given by

$$y^2 + z^2 = (b/a)^2(a^\nu - x^\nu)^{2/\nu}, \quad (3)$$

Manuscript received March 7, 1994; revised September 16, 1994.

The author is with the Physics Division, Research Department, Naval Air Warfare Center Weapons Division, China Lake, CA 93555-6001 USA.
IEEE Log Number 9408254.

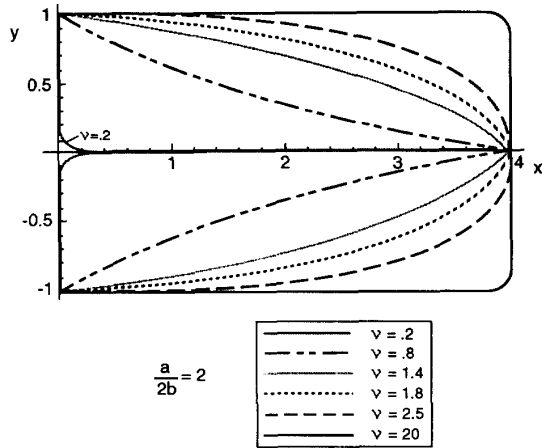


Fig. 1. Family of superspheroid cross sections in the xy plane ($z = 0, b = 1, a = 4$).

having a circular cross section in the yz plane and half of a superquadric cross section in the xz or xy planes. Immediately it is obvious, when $\nu = 2$, that (2) is the arc that will generate the right half of a prolate spheroid. In keeping with previous conventions [1], we will refer to the BOR's generated by (2) when $\nu \neq 2$ as *superspheroids*. We have found that these shapes are quite similar to traditional high speed missile radome shapes when appropriate values of a, b , and ν are used. The parameters b and a can be interpreted as the radome radius and length, respectively. The radome fineness ratio is given by $a/2b$. The planar cross section determined when $z = 0$ is an open boundary in the xy plane since x is allowed to run between 0 and a only. If some special cases of (3) are considered, we see that when $\nu = 1$, (3) is the equation of a cone (in cross section, a wedge) and when $\nu = 2$, (3) is half of a prolate spheroid (in cross section, half of an ellipse). When $1 < \nu < 2$, we obtain a family of radome cross sections appropriate for high speed missile applications with ν controlling their curvatures (see Fig. 1). If blunter nose shapes are desired, one can choose $\nu > 2$, while for pinched shapes, one uses $0 < \nu < 1$. The real value of the two-dimensional superquadric equation (1) or the superspheroidal equation (3) for radome applications lies in their simplicity. Analytically they are much easier to work with than the Von Karman or ogive equations [4]. Thus since these shapes are mathematically simple, it is possible to obtain closed form expressions for some of the geometric quantities associated with them, such as planar area [3], volume, etc. [5]. Usually this is not possible for traditional radome geometries.

In Section II, we will consider the tangent and normal vectors associated with superspheroids as well as formulas for the curvature and incidence angles since these quantities are necessary for many methods of radome analysis [4], [6]–[11]. In Section III we will compare the superspheroid family with traditional radome geometries and show that a number of traditional shapes can be well approximated by superspheroids using appropriate values for a, b , and ν . In Section IV, we use a ray tracing technique to obtain boresight error curves as functions of gimbal angle for various superspheroid geometries. Section V contains our conclusions.

II. TANGENTS, NORMALS, AND INCIDENCE ANGLE MAPS

Considering the arc in the first quadrant of the xy plane where $y = f(x) \geq 0$ for $0 \leq x \leq a$, we find that the derivative of (2) is simply

$$f'(x) = -\frac{b}{a} x^{\nu-1} (a^\nu - x^\nu)^{(1/\nu)-1}. \quad (4)$$

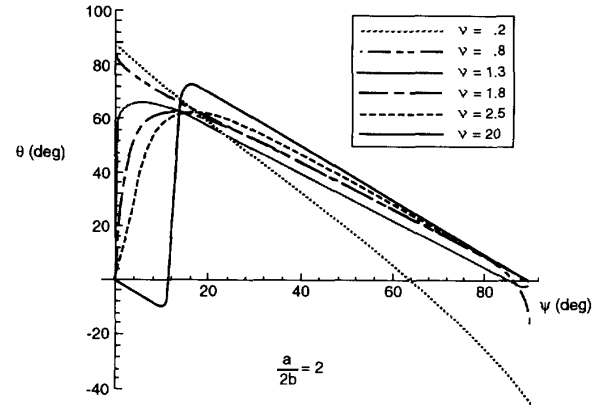


Fig. 2. Superspheroid incidence angle map for a 2-1 geometry using ν as a parameter.

Setting the antenna gimbal point at the coordinate origin, the equation of the central ray projected from the origin is just

$$y = x \tan \psi \quad (5)$$

where ψ is the antenna gimbal angle.

The x -coordinate of the point at which the central ray (or radius vector) intersects the superquadric is given by

$$x_i = \frac{ab}{[a^\nu (\tan \psi)^\nu + b^\nu]^{1/\nu}}. \quad (6)$$

The unit tangent vector to the superquadric is

$$\hat{t} = \frac{a(a^\nu - x^\nu)^{1-(1/\nu)}\hat{x} - bx^{\nu-1}\hat{y}}{\{a^2(a^\nu - x^\nu)^{2-(2/\nu)} + b^2x^{2(\nu-1)}\}^{1/2}} \quad (7)$$

and the unit normal is

$$\hat{n} = \frac{bx^{\nu-1}\hat{x} + a(a^\nu - x^\nu)^{1-(1/\nu)}\hat{y}}{\{a^2(a^\nu - x^\nu)^{2-(2/\nu)} + b^2x^{2(\nu-1)}\}^{1/2}}. \quad (8)$$

Thus the incidence angle, θ , is given by either

$$\cos \theta = (\hat{r} \cdot \hat{n}) \quad (9a)$$

or

$$\sin \theta = (\hat{r} \cdot \hat{t}) \quad (9b)$$

where the unit radius vector, \hat{r} has been written in the form

$$\hat{r} = \frac{\hat{x} + \tan \psi \hat{y}}{\sqrt{1 + \tan^2 \psi}}. \quad (10)$$

Dividing (9b) by (9a) and substituting (6) into \hat{n} and \hat{t} , we obtain a convenient form for the incidence angles of superquadric shapes in the xy plane as a function of the antenna gimbal angle, i.e.,

$$\tan \theta = \frac{[a^{2\nu} (\tan \psi)^\nu]^{1-(1/\nu)} - b^\nu a^{\nu-2} \tan \psi}{\tan \psi [a^{2\nu} (\tan \psi)^\nu]^{1-(1/\nu)} + b^\nu a^{\nu-2}}. \quad (11)$$

Note that for $\nu = 2$, i.e., half of an ellipse, formula (11) reduces to

$$\tan \theta = \frac{a^2 - b^2}{a^2 \tan \psi + b^2 \cot \psi} \quad (12)$$

as given in [4]. Plotting (11), Fig. 2 shows incidence angle maps for a given fineness ratio and different values of ν .

In some radome analysis methods, attempts have been made to take curvature directly into account [12]–[13]. In such methods, it is often helpful to know the principal radii of curvature. The first

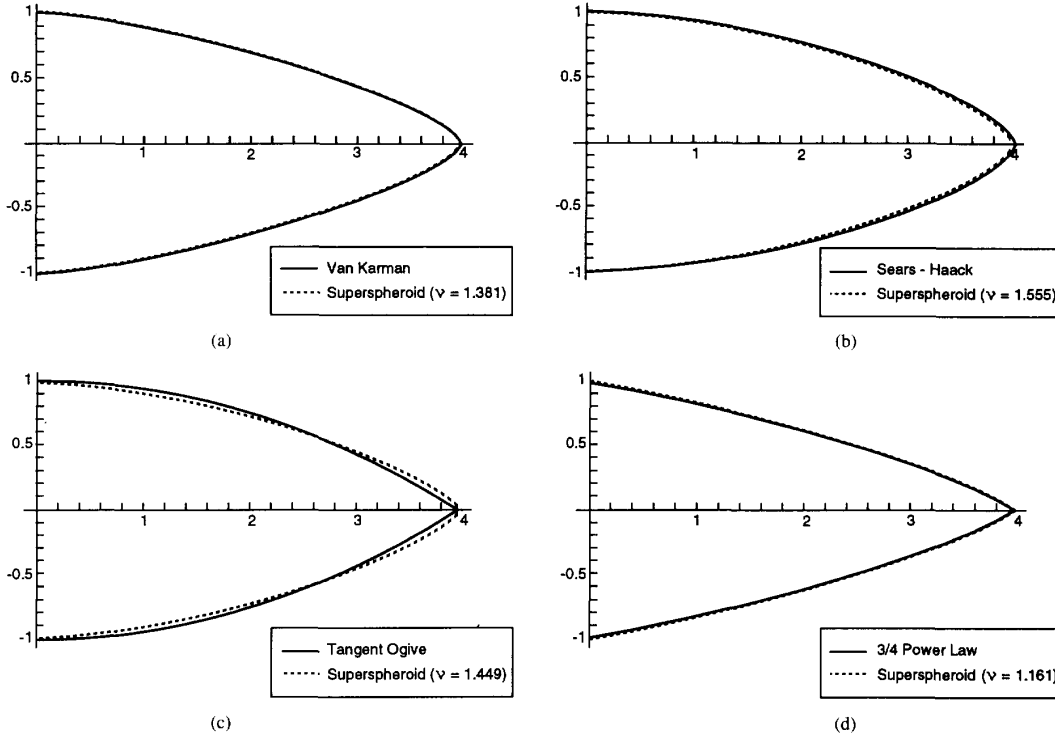


Fig. 3. (a) Comparison between a Von Karman and a superspheroid geometry ($D = 2, l = 4, \kappa = 0; a = 4, b = 1, \nu = 1.381$). (b) Comparison between a Sears-Haack and a superspheroid geometry ($D = 2, l = 4, \kappa = 1/3; a = 4, b = 1, \nu = 1.555$). (c) Comparison between a tangent ogive and a superspheroid geometry ($b_a = 1, R = 8.5; a = 4, b = 1, \nu = 1.449$). (d) Comparison of a three-quarter power law and a superspheroid geometry ($D = 2, l = 4, m = 0.75; a = 4, b = 1, \nu = 1.161$).

and second principal radii of curvature are given by the standard formulas [14]–[15]

$$R_1 = \frac{[1 + f'(x)^2]^{3/2}}{f''(x)}, \quad R_2 = -f(x)[1 + f'(x)^2]^{1/2} \quad (13)$$

or for the superspheroids (see (14), shown at the bottom of the page) while

$$R_2 = -\frac{b}{a}(a^\nu - x^\nu)^{1/\nu} \left[1 + \left(\frac{b}{a} \right)^2 x^{2(\nu-1)} \cdot (a^\nu - x^\nu)^{((2/\nu)-2)} \right]^{1/2}. \quad (15)$$

When the value of ν is 2, the formulas for R_1 and R_2 reduce to those for a spheroidal surface given in [14].

Also, the superspheroids possess the quality of similarity [16], meaning that one can obtain curves from the superspheroid equation that are exactly the same in form and that differ only in scale. For example a simple generalization of (1) in the xy plane is

$$\left(\frac{x}{a} \right)^\nu + \left(\frac{y}{b} \right)^\nu = \eta \quad (16)$$

where η is any constant. This automatically causes the a and b parameters to scale to

$$\frac{x^\nu}{\eta a^\nu} + \frac{y^\nu}{\eta b^\nu} = 1 \quad (17)$$

or the new a and b are $a' = a\eta^{1/\nu}$, $b' = b\eta^{1/\nu}$. Thus we can use (16) to obtain “nested” or similar superquadrics where the fineness ratio of each shape is $(a/2b) = (a'/2b')$ and is independent of η . This quality is not always present (or if present is not always obvious) in the equations describing traditional radome geometries.

III. APPROXIMATION OF TRADITIONAL RADOME SHAPES USING SUPERSPHEROIDS

In this section, we compare the equations describing the Von Karman, Sears-Haack, tangent ogive, and power law radomes with superspheroidal approximations. Beginning with the Von Karman geometry, we use the Haack-Von Karman equation in the xy plane [4]–[7],

$$y^2 = \frac{D^2}{4\pi} \left[\zeta - \frac{1}{2} \sin 2\zeta + \kappa \sin^3 \zeta \right] \quad (18)$$

where

$$\zeta = \cos^{-1} \left(\frac{2x}{l} - 1 \right) \quad (19)$$

$$R_1 = \frac{\left\{ a^{1-\nu} x^{2-\nu} (a^\nu - x^\nu)^{(2-(1/\nu))} \left[1 + \left(\frac{b}{a} \right)^2 x^{2(\nu-1)} (a^\nu - x^\nu)^{((2/\nu)-2)} \right]^{3/2} \right\}}{b(1-\nu)} \quad (14)$$

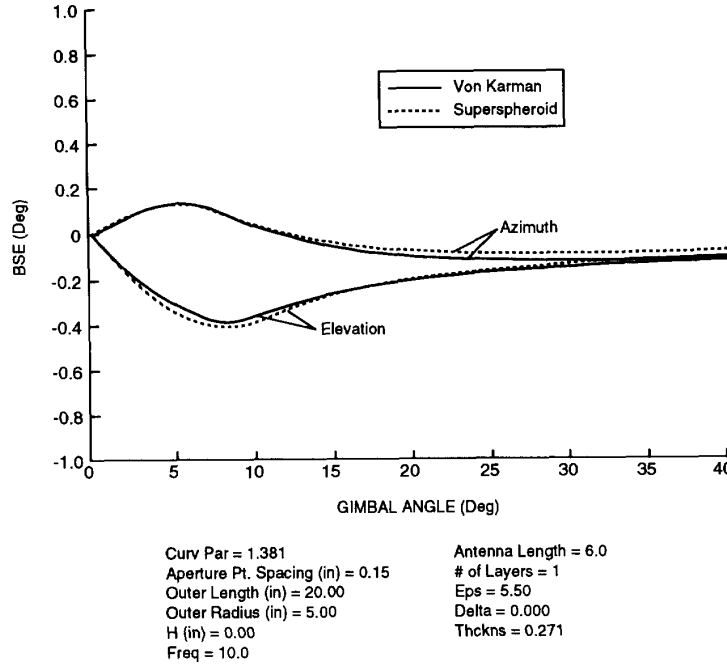


Fig. 4. Comparison of BSE induced by Von Karman and induced by superspheroid radome as a function of gimbal angle.

TABLE I

Shape	Optimum ν	Minimum $\ f - g\ $
Von Karman	1.381	0.00915
Tangent Ogive	1.449	0.06756
Sears-Haack	1.555	0.02523
Power Law ($m = \frac{3}{4}$)	1.161	0.03012

and κ is a constant, D is the diameter, and l is the total length of the radome. When the constant κ is equal to zero, we have a Von Karman shape. When κ is equal to one-third, we have a Sears-Haack shape. Both of these geometries have been very successful in radome design due mainly to their aerodynamic properties [4].

In attempting to approximate the traditional radome shapes with superspheroids, we have used the distance between two curves, $f(x)$ and $g(x)$, given by [17]

$$\|f - g\| = \left\{ \int_0^a [f(x) - g(x)]^2 dx \right\}^{1/2} \quad (20)$$

as a measure of how "good" the approximation is. Equation (20) is a functional of the least-squares type and is the simplest possible functional which yields an accurate positive definite residual [18]. Thus by minimizing $\|f - g\|$, and choosing fixed values for a and b we can find that value of ν which corresponds to the minimum of $\|f - g\|$. This value of ν is then optimum in providing the "best" approximation of $g(x)$ to $f(x)$ in the least-squares sense. Table I gives the optimized values of ν , which result in the best least-squares approximation of the superspheroid geometry to the Von Karman, tangent ogive, Sears-Haack and power law radome contours. The optimum value of ν is not affected by changes in the radome fineness ratio.

Fig. 3(a) shows a comparison between a Von Karman shape with $D = 2$, $l = 4$, $\kappa = 0$, and a superspheroid with $a = 4$, $b = 1$, $\nu = 1.381$. We have found that these two geometries are indistinguishable

graphically over a range of ν where $1.34 < \nu < 1.40$. Thus the approximation of the Von Karman by a superspheroid is not very sensitive to changes in the ν parameter. When κ is equal to one-third, (18) describes a Sears-Haack radome shape. Fig. 3(b) shows a comparison between the Sears-Haack geometry with $D = 2$, $l = 4$, and a superspheroid with $b = 1$, $a = 4$, $\nu = 1.555$. As for the Von Karman shape, the difference between the superspheroid and Sears-Haack is indistinguishable graphically.

Comparison between a tangent ogive and a superspheroid is shown in Fig. 3(c). The ogive defining equation in the xy plane is

$$y^2 = (\sqrt{R^2 - x^2} + b_a - R)^2 \quad (21)$$

where b_a is the base radius and R is the radius of the "parent circle" which traces out the shape. The tangent ogive is much harder to approximate using a superspheroid than the Von Karman or Sears-Haack shapes.

In Fig. 3(c), we have chosen $b_a = 1$, $R = 8.5$ for the tangent ogive, and $a = 4$, $b = 1$, and $\nu = 1.449$ for the approximating superspheroid. This value of ν causes the two geometries to match in an overall sense but with significant differences near $x = 1$ and $3 \leq x \leq 4$. Although the two curves are quite distinguishable graphically, for many numerical purposes, the approximation of a tangent ogive by a superspheroid (with $\nu = 1.449$) would be acceptable.

The set of previously known shapes which is closest analytically to the superspheroids is the set of power law shapes [4]. They are defined in the xy plane by

$$y = \frac{D}{2} \left(\frac{l - x}{l} \right)^m \quad (22)$$

where D is the base diameter, l is the length, and m is a constant. In its three-dimensional form, when m is one-half we obtain a paraboloid, and when m is one, (22) defines a cone. The most famous

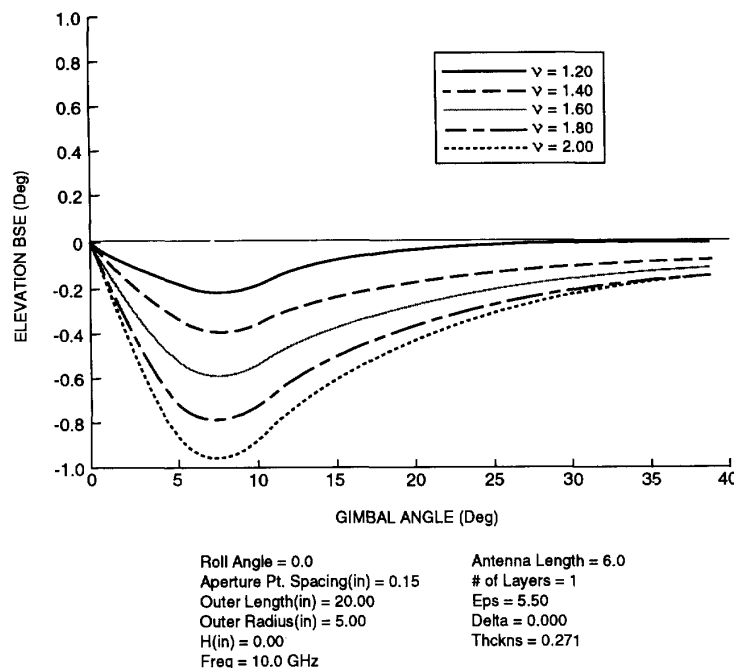


Fig. 5. BSE versus gimbal angle for 2-1 fineness ratio single layer superspheroid radomes ($1.2 \leq \nu \leq 2$).

of this set of shapes is the three-quarter power law ($m = 0.75$) which is itself an approximation to a true Newtonian shape.

Fig. 3(d) compares the three-quarter power law shape with a superspheroid where $D = 2$, $l = 4$, $m = 0.75$, and $a = 4$, $b = 1$, $\nu = 1.161$. As for the Von Karman and Sears-Haack contours, the three-quarter power law shape and the superspheroid are again graphically indistinguishable when the optimum ν is used. While the power law shapes are analytically as simple as the superspheroids, they are unable to approximate the Von Karman, Sears-Haack, or tangent ogive geometries as well as do the superspheroid family.

IV. BORESIGHT ERROR OF THE SUPERSPHEROIDS USING RAY TRACING

Using a ray tracing computer program developed at the Naval Air Warfare Center Weapons Division, China Lake, CA [6], we are able to evaluate the performance of the superspheroid family of radome shapes in terms of boresight error (BSE). The figures in this section show the BSE as a function of gimbal angle with ν as a parameter for a set of superspheroids with 2 to 1 fineness ratio. We have assumed a single layer of thickness $\lambda/2$ and $\epsilon = 5.5$ (pyroceram). The antenna is linearly polarized along the \hat{y} axis such that the elevation plane corresponds to the E-plane and the azimuth plane corresponds to the H-plane. Also we have used the convention that positive BSE points toward the nose and negative BSE points away from the nose. First, Fig. 4 compares the BSE in both elevation and azimuth planes from a Von Karman radome with that from a corresponding superspheroid with $\nu = 1.381$. As expected from the closeness of the geometric shape approximation, their BSE curves are extremely close. Then Fig. 5 indicates the BSE behavior of the superspheroids as a function of gimbal angle for various ν values. For a fixed fineness ratio and $1.2 \leq \nu \leq 2$, we see that typical BSE curves result with the smallest error occurring at $\nu = 1.2$, the largest at $\nu = 2$. Thus for this particular case, a more conically shaped radome provides better (less) BSE than does a more elliptically shaped dome.

V. CONCLUSIONS

We have used the two-dimensional superquadric equation in the first quadrant and revolved it about its major axis to obtain a body of revolution family of geometric shapes called superspheroids. For certain values of length and radius and assuming that $1 < \nu < 2$, we have determined shapes appropriate for high speed missile radomes. We have found that the superspheroid characterized by the curvature parameter $\nu = 1.381$ is an almost exact match for the Von Karman shape. We have determined incidence angle maps, geometric properties, and used ray tracing to obtain boresight error as a function of gimbal angle for the superspheroids. This family of shapes is mathematically simple, can approximate most of the traditional radome geometries quite well, and is exceptionally easy to either program or use analytically.

ACKNOWLEDGMENT

The author would like to thank B. M. Ryan, formerly of DCS Corporation and D. J. White of Comarco, Inc., for helpful technical discussion. The author is very grateful to the Naval Sea Systems Command for continued financial support. Also the author thanks an unknown reviewer for a number of helpful suggestions.

REFERENCES

- [1] A. H. Barr, "Superquadrics and angle preserving transformations," *IEEE Computer Graph. Appl.*, vol. 1, Jan. 11-23, 1981.
- [2] E. D. Constantinides and R. J. Marhefka, "Plane wave scattering from 2-D perfectly conducting superquadric cylinders," *IEEE Trans. Antennas Propagat.*, vol. 39, pp. 367-376, Mar. 1991.
- [3] D. W. Duan and Y. Rahmat-Samii, "Reflector antennas with superquadric aperture boundaries," *IEEE Trans. Antennas Propagat.*, vol. 41, pp. 1164-1167, Aug. 1993.
- [4] T. E. Tice and J. D. Walton, Eds., *Techniques for Airborne Radome Design, Vols. I and II*. Albuquerque, NM: Air Force Weapons Laboratory, Technical Report AFAL-TR-66-391, Dec. 1966.

- [5] P. L. Overfelt, *Superspheroid Geometries for Radome Analysis*. China Lake, CA: Naval Air Warfare Center Weapons Division, Technical Publication 8216, Aug. 1994.
- [6] —, *Computer Codes for Electromagnetic Design and Analysis of Radomes*. China Lake, CA: Naval Weapons Center, Technical Publication 6598, Mar. 1985.
- [7] P. L. Overfelt, C. S. Kenney, D. J. White, and W. O. Alltop, *Radome Analysis and Design Tool (Final Report)*. China Lake, CA: Naval Air Warfare Center Weapons Division, Technical Publication 8171, Nov. 1993.
- [8] P. L. Overfelt, "Two-dimensional radome modelling: A boundary perturbation approach," in *1984 IEEE Int. Symp. Dig. Antennas Propagat.*, June 1984, pp. 201–205.
- [9] P. L. Overfelt and D. J. White, "Electromagnetic analysis of radomes using a spherical wave point dipole source array technique," in *21st Symp. Electromagnetic Windows Dig.*, Sept. 1988, pp. 11–25.
- [10] D. C. F. Wu and R. C. Ruddock, "Plane wave spectrum-surface integration technique for radome analysis," *IEEE Trans. Antennas Propagat.*, vol. AP-22, pp. 497–500, May 1974.
- [11] K. Siwiak, T. B. Dowling, and L. Lewis, "Boresight errors induced by missile radomes," *IEEE Trans. Antennas Propagat.*, vol. AP-27, pp. 832–841, Nov. 1979.
- [12] J. H. Chang and K.-K. Chan, "Analysis of a two-dimensional radome of arbitrarily curved surface," *IEEE Trans. Antennas Propagat.*, vol. 38, pp. 1565–1568, Oct. 1990.
- [13] X. J. Gao and L. B. Felsen, "Complex ray analysis of beam transmission through two-dimensional radomes," *IEEE Trans. Antennas Propagat.*, vol. AP-33, pp. 963–975, Sept. 1985.
- [14] C. T. Tai, *Generalized Vector and Dyadic Analysis*. New York: IEEE Press, 1992.
- [15] D. J. Struik, *Differential Geometry*. Cambridge, MA: Addison-Wesley, 1950.
- [16] A. G. Hansen, *Similarity Analyses of Boundary Value Problems in Engineering*. Englewood Cliffs, NJ: Prentice-Hall, 1964.
- [17] J. M. H. Olmsted, *Advanced Calculus*. New York: Appleton, Century, Crofts, 1961, ch. 16.
- [18] M. Becker, *The Principles and Applications of Variational Methods*. Cambridge, MA: MIT Press, 1964, ch. 3.

Imaginary Part of Antenna's Admittance from its Real Part Using Bode's Integrals

Smain Amari, Martin Gimersky, and Jens Bornemann

Abstract—The imaginary part of an antenna input admittance is calculated from its real part using Bode's integrals. Since the real part is typically a smoother function of the frequency than the imaginary part, the procedure presented here requires computation at a smaller number of frequency points, thus saves time, and is ideal for systems whose input conductance exhibits sharp peaks. A numerical procedure to evaluate the singular Bode's integral is also presented. Numerical examples using a wire antenna are used to illustrate the advantages of this approach compared to calculations involving a densely scanned frequency range. The noise stability and robustness of the algorithm are demonstrated through the successful prediction of the susceptance and the resonant frequencies of the antenna in the presence of random noise in the conductance.

I. INTRODUCTION

The integral relations between real and imaginary parts of response functions are widely used in quantum field theory, nuclear physics,

and solid state physics. Unfortunately, this extremely useful tool does not seem to find much use in microwave engineering.

These integral relations are known under a variety of names. The Kramers–Kronig relations between the real and imaginary parts of the dielectric constants are well known to engineers and physicists. In quantum field theory and quantum many-body theory, they are sometimes known as Lehmann or spectral representations or dispersion relations [1], whereas mathematicians refer to them as Hilbert Transforms. In circuit theory, they are often called Bode's integrals, since Bode seems to have been the first to use them [2].

Kramers–Kronig relations enjoyed substantial popularity in the sixties among researchers in optics, where it is possible to measure the imaginary part since it is related to light (electromagnetic) absorption [3]. Once the imaginary part is known, these relations are used to calculate the real part. Such relations also provide a set of constraints on the moments of the functions involved as well as their asymptotic behavior and are very useful tools to check the numerical accuracy of the calculations [2], [4].

One of the most intensive numerical problems in modern antenna analysis and design is the accurate calculation of the resonant frequency, especially for antennas with sharply peaked input conductance. For such antennas, the imaginary part of the admittance oscillates violently around the resonant frequency, thereby requiring its evaluation at a very large number of frequency points in order to accurately predict the location of the resonance. Although empirically derived formulas for admittances and resonant frequencies of certain types of antennas exist, they are of low accuracy (e.g., $\pm 20\%$ for helices [5]) or not known at all for other structures such as those involving anisotropic and lossy materials [6]. For all of these systems, however, the real part of the input admittance, although having sharp peaks, is much easier to describe than its imaginary part, hence requiring fewer computations around the peak which can locally be approximated by a Lorentzian.

Fortunately, it is for these numerically demanding situations that Bode's integrals will be shown to work best. Indeed, the presence of a sharp peak in the real part determines the local behavior of the imaginary part because of the singularity in the integrand. Thus it is possible to reliably predict the resonant frequency and susceptance from the real part without accurately reproducing the entire frequency dependence of the susceptance.

Since the presence of a Cauchy Principal-Value in these integral relations poses a numerical problem, which should be handled with care, a numerical procedure using cubic splines to calculate these integrals is presented. It is similar to the modified Simpson rules presented in [7] but, we feel, is more appropriate for real life quantities which are expected to be smooth functions.

The paper is organized as follows. In Section II we briefly review Bode's integrals. Section III presents a numerical procedure based on a cubic-spline interpolation to calculate the singular integrals involved. In Section IV, we apply the method to calculate the susceptance of a wire antenna as a function of frequency from its real part. The obtained results are compared with those obtained from a direct method-of-moments solution. In Section V, the noise stability of the present technique is investigated using a randomly generated error in the real part to simulate measurement errors. It is shown that the first resonant frequency is adequately predicted despite the presence of the corrupting noise.

II. BODE'S INTEGRALS

The derivation of Bode's integrals is not presented here, the reader is referred to the literature for the details [2], [3], [8]. We only

Manuscript received July 1, 1994; revised October 12, 1994.

The authors are with the Department of Electrical and Computer Engineering, University of Victoria, Victoria, B.C., Canada V8W 3P6.

IEEE Log Number 9408257.